

PDF hosted at the Radboud Repository of the Radboud University Nijmegen

The following full text is a publisher's version.

For additional information about this publication click this link.

<http://hdl.handle.net/2066/198261>


Please be advised that this information was generated on 2019-06-02 and may be subject to change.

SCIENTIFIC REPORTS



OPEN

Csde1 binds transcripts involved in protein homeostasis and controls their expression in an erythroid cell line

Kat S. Moore¹, Nurcan Yagci¹, Floris van Alphen², Nahuel A. Paolini¹, Rastislav Horos³, Ntsiki M. Held⁴, Riekelt H. Houtkooper⁴, Emile van den Akker¹, Alexander B. Meijer^{2,5}, Peter A. C. 't Hoen⁶  & Marieke von Lindern¹

Expression of the RNA-binding protein Csde1 (Cold shock domain protein e1) is strongly upregulated during erythropoiesis compared to other hematopoietic lineages. Csde1 expression is impaired in the severe congenital anemia Diamond Blackfan Anemia (DBA), and reduced expression of Csde1 in healthy erythroblasts impaired their proliferation and differentiation. To investigate the cellular pathways controlled by Csde1 in erythropoiesis, we identified the transcripts that physically associate with Csde1 in erythroid cells. These mainly encoded proteins involved in ribogenesis, mRNA translation and protein degradation, but also proteins associated with the mitochondrial respiratory chain and mitosis. Crispr/Cas9-mediated deletion of the first cold shock domain of Csde1 affected RNA expression and/or protein expression of Csde1-bound transcripts. For instance, protein expression of Pabpc1 was enhanced while *Pabpc1* mRNA expression was reduced indicating more efficient translation of Pabpc1 followed by negative feedback on mRNA stability. Overall, the effect of reduced Csde1 function on mRNA stability and translation of Csde1-bound transcripts was modest. Clones with complete loss of Csde1, however, could not be generated. We suggest that Csde1 is involved in feed-back control in protein homeostasis and that it dampens stochastic changes in mRNA expression.

RNA binding proteins (RBP) regulate transcript stability and translation. RBPs can cooperate with protein complexes of the general mRNA translation machinery, or with protein complexes that control mRNA location and/or degradation. Deregulated expression of such RBPs affects protein synthesis from a set of transcripts particularly dependent on that specific RBP. This has been referred to as an RNA regulon¹. The RNA regulon may be cell-type specific, because it depends on the available transcriptome in these cells. The RNA regulon may also define a set of ubiquitously expressed transcripts whose translation is modified by cell type specific expression of RBP. For instance, hematopoietic stem- and progenitor cells (HSPC) express the RBP Musashi-2, which is crucial for maintenance and repopulation ability of the HSPC². The RBP Znf3612 (Zinc finger protein 36-like 2), a member of the Tristetraproline family, is expressed in early erythroblasts and mediates glucocorticoid-mediated expansion of the erythroid compartment³. We observed that the RBP Csde1 is strongly upregulated in expanding erythroblasts (>100-fold) compared to other hematopoietic cell types⁴. In Diamond Blackfan Anemia (DBA), a ribosomopathy due to haploinsufficiency of ribosomal proteins, this upregulation was impaired⁴. This raised our interest in the role of Csde1 in erythropoiesis.

Csde1 was first described as Unr (upstream of N-ras) in *Drosophila melanogaster*⁵. It binds an AG-rich domain in the 3'UTR of *Msl* (*Male sex lethal*) and suppresses translation^{6,7}. Its expression is highly conserved across species and Csde1 binds its own IRES to repress translation in mammalian cells⁸. Csde1 also enhances

¹Department Hematopoiesis, Sanquin, and Landsteiner Laboratory AMC/UvA, 1066 CX, Amsterdam, The Netherlands. ²Department of Plasma proteins, Sanquin Research, 1066 CX, Amsterdam, The Netherlands. ³European Molecular Biology Laboratory, 69117, Heidelberg, Germany. ⁴Laboratory Genetic Metabolic Diseases, Academic Medical Center, 1105 AZ, Amsterdam, The Netherlands. ⁵Department of Biomolecular Mass Spectrometry and Proteomics, Utrecht Institute for Pharmaceutical Sciences, Utrecht University, Utrecht, The Netherlands. ⁶Center for Human and Clinical Genetics, Leiden University Medical Center, 2300 RC, Leiden, The Netherlands. Correspondence and requests for materials should be addressed to M.v.L. (email: m.vonlindern@sanquin.nl)

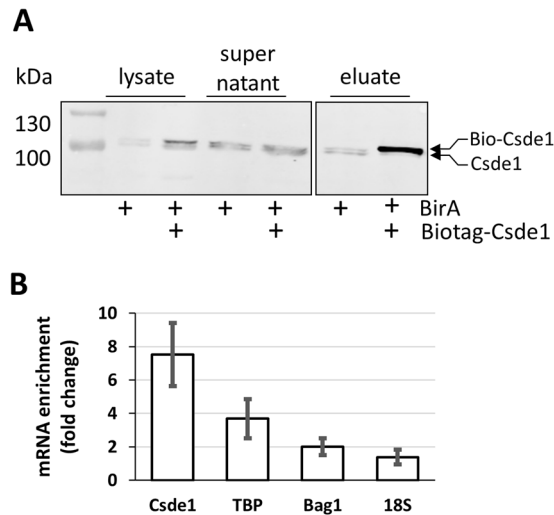


Figure 1. Purification of Csde1 containing RNP complexes. **(A)** MEL cells expressing BirA, or expressing BirA plus biotag-Csde1 were lysed, and incubated with streptavidin beads. Supernatant and beads were collected, beads were washed and eluted. Western blot with fractions was stained with anti-Csde1 antibody. Size markers are indicated in kDa. The positions of endogenous and biotagged Csde1 are indicated. A single empty lane has been cropped. The uncropped image is available as Supplementary Figure S5. **(B)** RNA was isolated from eluates and tested for expression of *Csde1*, *Tbp* (*Tata binding protein*), *Bag1* and *18S* RNA by Q-PCR. The fold-change enrichment of the transcripts on streptavidin beads incubated with biotag-Csde1 lysate was calculated compared to pull downs from BirA MEL cells (error bars indicate SD, n = 3).

IRES-dependent translation of select transcripts, such as *Apaf1* (*apoptotic peptidase activating factor 1*)⁹ and *Cdk11B* (*cyclin dependent kinase 11B*)^{10,11}. Overall, the role of Csde1 in control of mRNA stability and translation may be diverse as it binds transcripts through distinct sites^{12,13}.

The diverse effects of Csde1 on bound transcripts may be explained by the RNA context and by the associated proteins that control the RNA binding affinity. Csde1 cooperates with PTB and hnRNP C1/C2 to control IRES-dependent translation of *Apaf1* and *Cdk11B*, respectively^{6,11,14}, it cooperates with DDX6 and miRNA in translational repression and P-body assembly¹⁵, and it acts together with Pabp to control mRNA translation and stability through elements in the 3'-UTR of specific transcripts^{16,17}. Increased expression of Csde1 has been associated with melanoma and breast cancer^{18,19}. Analysis of Csde1-bound transcripts in melanoma implied Csde1 in control of metastasis as it bound to, and increased expression of, for instance, Vimentin¹⁸.

Csde1 expression is much increased in erythroblasts compared to other hematopoietic cells, and reduced expression in primary mouse erythroblasts impaired their proliferation and differentiation similar to knock down of ribosomal proteins⁴. Thus, Csde1 controls important erythroblast functions that must differ from previously described functions such as sex specification or migration during metastasis. To identify its function in erythropoiesis, we aimed to identify the transcripts that are bound by Csde1 in erythroblasts, and to evaluate the effect Csde1 on transcript stability and translation. Csde1-bound transcripts mainly encoded proteins involved in protein homeostasis, ranging from ribosome biosynthesis, translation, to protein degradation. In addition, Csde1 bound transcripts encoding proteins involved in mitosis. Protein homeostasis and mitosis are affected in DBA. Csde1 also reduced translation of several ribogenesis factors, and increased translation from reduced Pabpc1 transcript levels. Overall, we suggest that the function of Csde1 is involved in feed-back control during protein homeostasis and that it may dampen stochastic changes in gene expression.

Results

Pull down of Csde1-bound transcripts. To identify mRNA transcripts bound by Csde1, we expressed *in vivo* biotinylated Csde1 in erythroid cells. MEL cells expressing the prokaryotic biotin ligase BirA were transfected with a *Csde1* construct tagged with the recognition site of BirA. Tagged and endogenous Csde1 were expressed at comparable levels⁴. RNA-protein complexes containing Biotag-Csde1 were precipitated on streptavidin beads (Fig. 1A). Two bands were visible when blots were stained with anti-Csde1, also when the cells did not express tagged Csde1. Ribosome footprint analysis performed in a parallel project revealed an alternative translation start site and the existence of an additional protein isoform with 11 additional upstream amino acids (Supplementary Figure S1). In addition, exon 5 (32 codons) is alternatively spliced, and ribosome footprinting suggests moderate translation of exon 5 compared to neighbouring exons 3 and 4 (Supplementary Figure S1). The shorter, annotated form of Csde1 was fused to the 13nt biotag and therefore appeared of the same size as either the extended alternative protein isoform or the longer isoform encoded by the transcript containing exon 5. Streptavidin beads specifically associated with biotag-Csde1 (Fig. 1A). As Csde1 binds the IRES in its own transcript, we used conditions that enriched for binding to Csde1 mRNA, using *Bag1*, *Tbp* (*TATA-binding protein*) or *18S* rRNA as background signals (Fig. 1B).

Identification of Csd1-bound transcripts. Streptavidin binding protein/RNA complexes were harvested from the cytoplasmic lysate of BirA expressing MEL cells that did or did not co-express biotag-Csd1. We isolated and processed RNA from three independent samples for sequence analysis with Illumina MiSeq; one sample was sequenced separately together with one control. Principle component analysis (PCA) discriminated the samples on sequence run in PC1, whereas PC2 discriminated the transcripts pulled down in biotag-Csd1/BirA expressing MEL cell lysates from the transcripts harvested from BirA control cell lysates (Fig. 2A). To identify the transcripts that are significantly enriched in biotag-Csd1-RNA complexes, we analyzed the results with DESeq2. Both significantly enriched and depleted transcripts were detected in Csd1-biotag/BirA MEL cells compared to BirA MEL cells, with a clear skewing towards enriched transcripts, as is to be expected during a pulldown (Fig. 2B, Supplementary Table S-II). The depleted transcripts represent the small set of constitutively biotinylated proteins²⁰ and Supplementary Table S-II). We selected transcripts enriched with a Benjamini-Hochberg false discovery rate (FDR) <0.05. This yielded a list with 292 unique transcripts enriched in Csd1-protein complexes (Supplementary Table S-III). Transcripts assigned to pseudogenes were included in this list because they may have a regulatory function by quenching RBP and miRNA.

Previous studies using SELEX identified Csd1 binding sites as [A/G]₅AAGUA[A/G], or [A/G]₇AAC[A/G]₂²¹. We performed a search for either of these consensus sites with a custom Python script using Biopython²². They were present in 20% of Csd1-bound transcripts (60 out of 274, we excluded double counting on pseudogenes) versus 26% in random transcripts (248 out of 685) (Fig. 2C, Supplementary Table III). Not only the presence, but also the distribution of putative binding sites between the protein coding region (13% and 16%) and the 3'UTR (8% and 11%) in Csd1-bound and random transcripts was comparable (Fig. 2C). Thus, the presence of a consensus Csd1 binding site as determined by SELEX in transcripts is not predictive for Csd1 binding. Notably, individual-nucleotide resolution UV crosslinking and immunoprecipitation (iCLIP) in melanoma cell lines identified a 6nt motif ([C/G/U]AAG[AUG]A)¹⁸. This short sequence can be found ubiquitously among all detected transcripts (data not shown), making it unsuitable for *in silico* analysis. Together, these studies suggest that the *in vivo* binding of Csd1 to its targets may be directed by its cellular context, more than the *in vitro* affinity of purified Csd1 to naked RNA sequences.

To identify the cellular processes that may be regulated by Csd1 in erythroblasts, we classified the transcripts according to functional groups (e.g. transcription, translation, mitochondrial function; Fig. 2D, Supplementary Table IV). To determine whether cellular processes are significantly enriched, we used Overrepresentation Analysis (ORA) with GeneTrail2²³ (Fig. 2D, Supplementary Table IV). Mitochondrion and mitochondrial respiration were highly enriched among the cellular component and biological process GO-terms, respectively (53 hits). This includes mitochondrial ribosomes and ribosome association (n = 23), the respiratory chain (n = 19), lipid synthesis (n = 3), heme synthesis (n = 3), mitochondrial membrane (n = 3) and transport of proteins to mitochondria (n = 2) (Fig. 2D). Abundantly represented were processes involved in mRNA translation (n = 74), including those associated with mitochondrial ribosomes (n = 23), ribosome biogenesis (n = 28), tRNA modifying enzymes (n = 9) and mRNA translation initiation and elongation (n = 14) (Fig. 2D). Also enriched were transcripts which affect protein synthesis via mRNA splicing (n = 16) and mRNA stability (n = 4). Csd1 targets additionally affect protein ability via maintenance of protein folding (n = 4), and via the activity of peptidases (n = 2), ubiquitinases (n = 9) and the proteasome (n = 10). The centrosome and control of mitosis were also significantly enriched terms (n = 11). Recent studies identified Csd1 targets in melanoma cells and *Drosophila melanogaster*^{18,24}. Comparison showed that 53 of the 274 transcripts we identified as Csd1-associated transcripts were also identified as a Csd1 target in melanoma cells using iCLIP¹⁸. These common transcripts encoded proteins that act in all cellular processes, but were particularly abundant in control of translation and ribogenesis (Fig. 2D, Supplementary Table S-IV).

Generating a model with reduced Csd1 expression. To investigate the role of Csd1 in expression and translation of Csd1-associated transcripts, we aimed to reduce the expression of Csd1 via shRNA transduction. Mass spectrometry revealed that lentiviral transduction *per se* strongly induced Csd1 expression, which was reduced to parental levels by Csd1-specific shRNAs. As an alternative to lentiviral knock-down, we used Crispr-Cas9²⁵ to generate deletions in Csd1 in MEL cells. Knock down of Csd1 in primary cells abrogated their proliferation and differentiation⁴. Therefore, we aimed for an in-frame deletion to remove the first cold shock domain, which causes a 20-fold reduction in RNA binding affinity^{20,26}. Guide RNAs in exon 3 (NM_144901.4), just downstream of the AUG start codon, and in exon 4 were transfected into MEL cells (Fig. 3A). Single cells were sorted by FACS (fluorescence assisted cell sorting) from the brightest, top 5%, of GFP-expressing cells. Selected clones were subsequently tested by PCR and Western blot for the intended deletion. In addition to heterozygous deletions, this yielded two clones with an out-of-frame Csd1 deletion (*Del*; shown are clones D1, D2), three hypomorph clones with the intended in-frame deletion (*Hm*; shown are clones H1, H2), and multiple clones with a mono-allelic out-of-frame deletion in addition to a wt allele (heterozygote deletions, *Het*, indicated as clones C1, C2) (Fig. 3B). It is noteworthy that the control-transfected clones expressed Csd1 protein similar to parental MEL cells. Clones H1 and H2 expressed a shorter Csd1 protein isoform, as expected (Fig. 3C). Surprisingly, clones D1 and D2 were expected to lose Csd1 expression, but anti-Csd1 antibody recognized proteins of 70–75 kDa (Fig. 3C).

Protein lysates of clones D1, D2, H1, H2, C1, C2 and wt MEL cells were submitted to mass spectrometry with label-free quantification. MaxQuant was used for peptide identification and quantification, and expression of Csd1 was verified²⁷. In accordance with Western blot data, Csd1 expression was similar in control clones and parental wt MEL cells, and reduced in clones H1 and H2 (Fig. 3D). Intriguingly, the out-of-frame deletion in the N-terminus of Csd1 was expected to abrogate Csd1 expression in clones D1 and D2, but Csd1 peptides were detected by mass spectrometry (Fig. 3D). Thus, both the Western blot and mass spectrometry suggested the expression of a shorter form of Csd1 in clones D1 and D2. Mapping the detected Csd1 peptides in the various

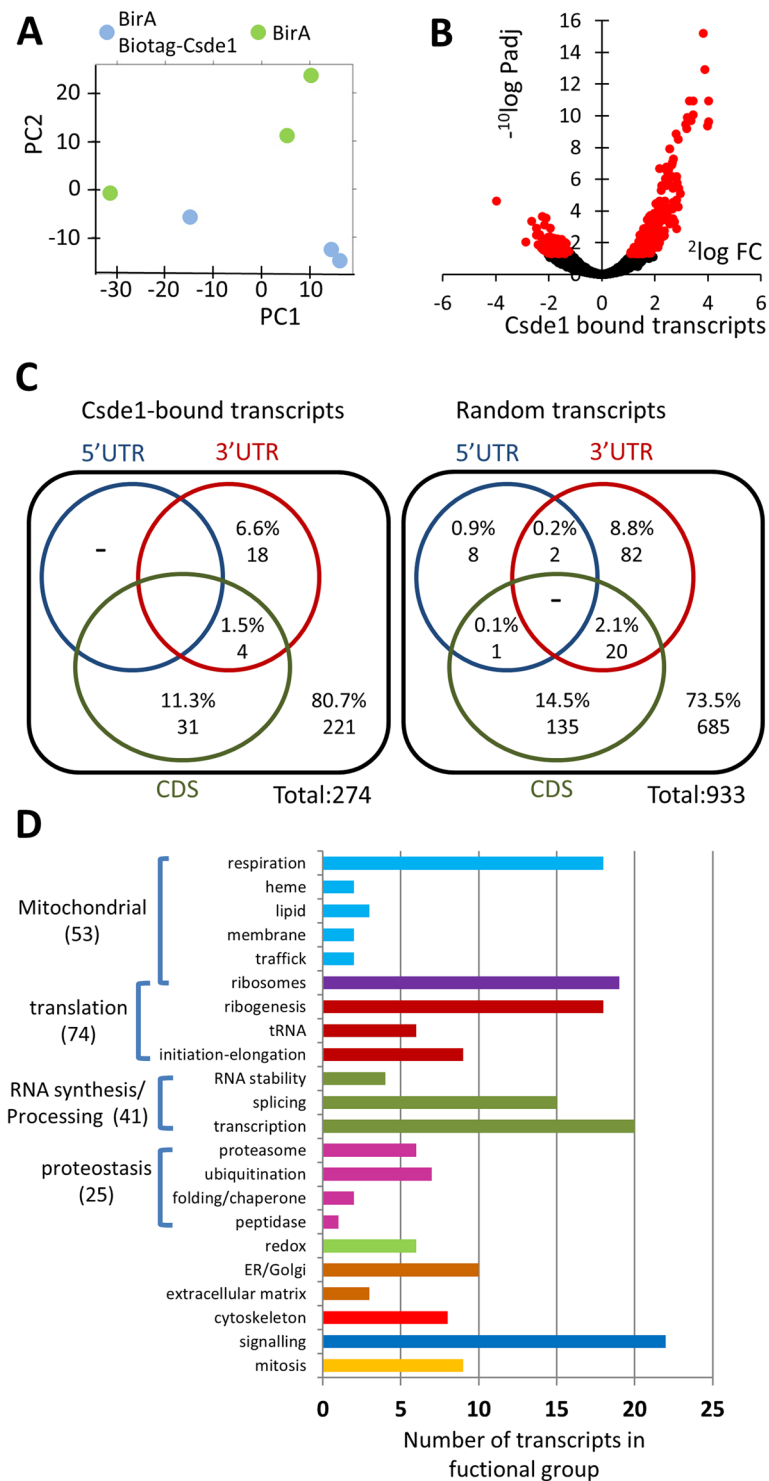


Figure 2. Identification of Csde1-bound transcripts. RNA was isolated from independent streptavidin bead eluates derived from MEL cells expressing BirA alone ($N = 3$), or BirA plus biotag-Csde1 ($N = 3$). RNA was sequenced, and differential abundance was analyzed by Deseq2. **(A)** Principle component analysis (green: BirA; blue BirA plus biotag-Csde1). **(B)** $-\log_{10}(\text{P-adjusted})$ plotted against $2\log(\text{fold change})$ of differentially enriched transcripts. Red: $\text{FDR} < 0.05$ **(C)** At $\text{FDR} < 0.05$ we identified transcripts from 274 unique genes (pseudogenes excluded) that associated with Csde1. Potential Csde1 binding sites ($[\text{A/G}]_5\text{AAGUA}[\text{A/G}]$, or $[\text{A/G}]_7\text{AAC}[\text{A/G}]_2$) are indicated (percentage and total number) for the 5'UTR (blue), protein coding region (CDS; red) and 3'UTR (green); for the 274 Csde1-bound transcripts, and for almost 1000 control transcripts. **(D)** Each transcript was assigned a unique label that best represented its function. The number of transcripts within a specific function are depicted (overarching functions in the same color).

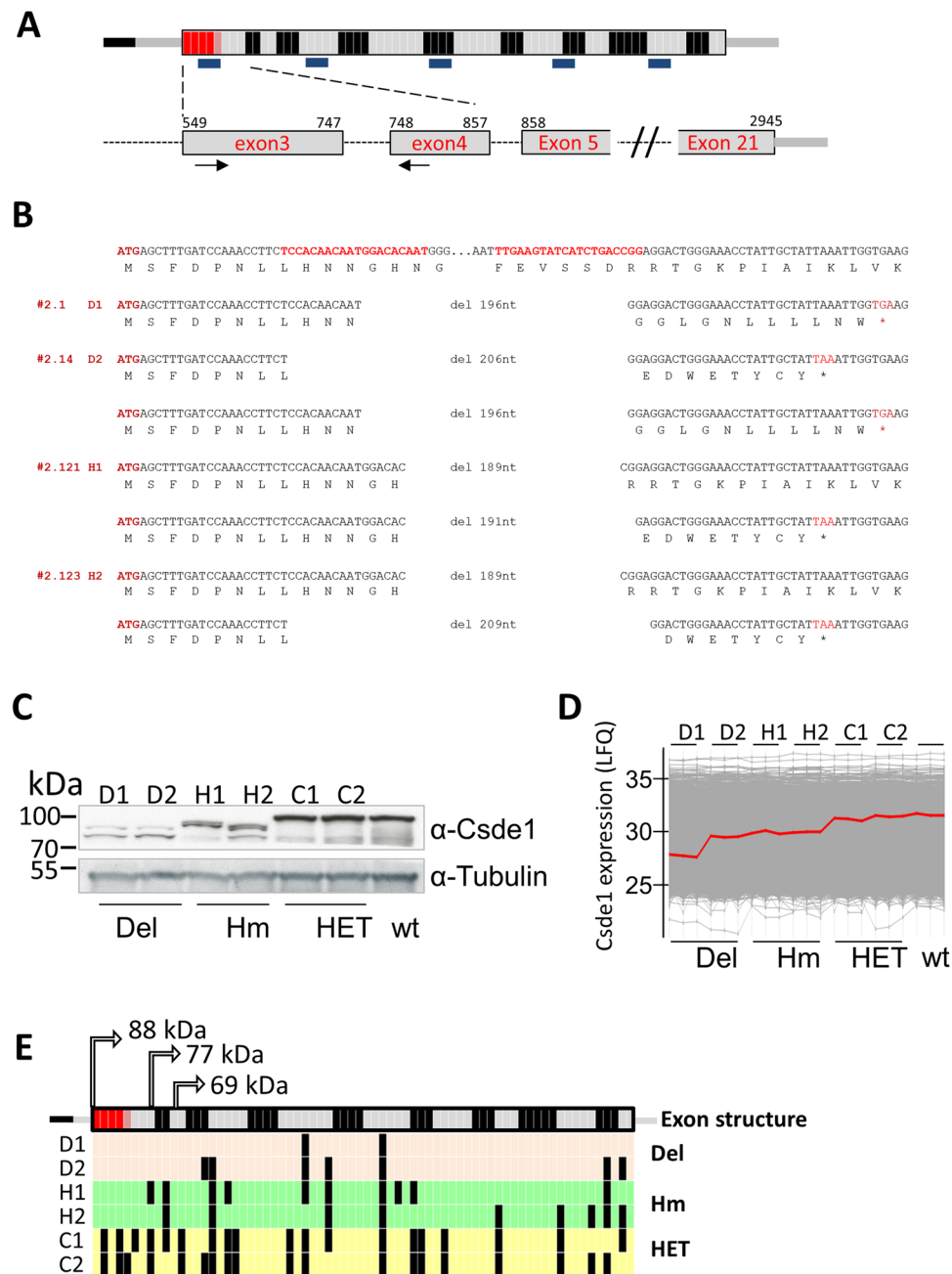


Figure 3. Deletion of the 1st cold shock domain of Csd1 using Crispr/Cas9. **(A)** Cartoon of the Csd1 transcript. Grey and black represent subsequent exons. Small squares represent individual tryptic peptides (exons and peptides in arbitrary size). Tryptic peptides were assigned to the exon that contributes most. The methionine start codon locates at the start of exon 3. The position of five cold shock domains is indicated by short bars below the transcript. Numbers on the zoom in on exons 3–5 indicate the nucleotide position of NM_144901.4. Guide RNAs are indicated with arrows, the red tryptic fragments are affected by the deletion. **(B)** The top sequence shows the guide RNAs in red, in their sequence context, and the amino acids below the codons. Below the sequence that reveals the precise deletion for both alleles in 4 clones, only 1 allele was detected in clone D1 (#2.1). **(C)** Western blot stained for Csd1 and tubulin as loading control. The membrane was cut between Csd1 and tubulin and staining performed on each separately. D1 (2.1) and D2 (2.14) represent out-of-frame deletions (Del), H1 (2.121) and H2 (2.123) in-frame deletions of the 1st cold shock domain (Hm). HET are control clones that harbor 1 deleted (out-of-frame) allele and 1 wt allele. Raw image scans are available as Supplementary Figure S6. **(D)** Mass spectrometry analysis with MaxQuant and Perseus yields a cartoon in which the protein expression of all proteins is indicated as LFQ by a grey line. Csd1 expression is indicated with a red line. **(E)** For Csd1, we identified 33 unique tryptic peptides. Black lines indicate tryptic fragments that were detected by mass spectrometry. Alternative AUG start codons that may explain truncated proteins are indicated by arrows, the size of the encoded protein in kDa.

clones identified 33 of 72 predicted tryptic peptides in parental MEL lines and in heterozygous deletion clones. (Fig. 3E). Several *Csde1* peptides were detected in clones D1 and D2 (Fig. 3E). These peptides were located downstream of the deletion, and downstream of a potential in frame start codon in exon 4. The number of peptides is too small to draw conclusions on the start site. In addition, the sequence of the predicted novel N-terminal tryptic peptides is too short to be specific. Ribosome footprints deposited in the GWIPS database (<http://gwips.ucc.ie/>)²⁸, indicate translation of several small uORFs in the 5'UTR of *Csde1*, which may facilitate leaky scanning and expression of smaller *Csde1* isoforms²⁹; Supplementary Figure 1).

The out-of-frame deletion in *Csde1* did not affect the proliferation of MEL cell clones D1 and D2 (data not shown). This is in contrast to the observed abrogation of proliferation in primary erythroblasts after *Csde1* knockdown⁴. Outgrowth of these clones was likely due to alternative translation initiation and expression of an N-terminally truncated *Csde1* protein. Notably, the in-frame deletion allows for expression of both the annotated and the extended *Csde1* isoform without cold shock domain 1. The out-of-frame deletion produces proteins only from downstream start codons.

The transcripts associated with *Csde1* were enriched for mRNAs encoding mitochondrial ribosomal proteins, and proteins of the mitochondrial respiratory chain. We investigated whether *Csde1* expression and function may control mitochondrial activity and capacity. *Csde1* was expressed in mitochondria, although at low expression levels (Supplementary Figure S2A). Mitochondrial respiration of Hm and Del clones was measured by Seahorse technology, but not altered in the Del and Hm clones compared to control clones (Supplementary Figure S2B).

Protein and RNA expression in Del and Hm *Csde1* mutant clones. Binding of *Csde1* to target transcripts may affect transcript stability and/or translation. Therefore, we examined both protein and RNA expression in the N-terminally truncated/deleted clones D1, D2, H1, H2, and in control clones C1, C2 and wt MEL parental cells. The peptide profiles of the two Del clones, the Hm clones, the control clones, and the parental BirA-MEL cells were subjected to cluster analysis. A total of 985 proteins were differentially expressed in any of the clones (ANOVA, *S0* cutoff 0.4, FDR cutoff 5%) (Supplementary Table V). The heatmap based on hierarchical clustering of relative protein expression data demonstrated that the two Hm clones cluster together and differ strikingly from both Del clones and from the control clones (Fig. 4A). The Del clones, which express *Csde1* proteins lacking the N-terminus, are more closely related the control clones, but both clones share a common gene expression program that is clearly different from control clones (Fig. 4A).

For 222 of the 274 *Csde1*-associated transcripts, we detected peptides at least in all Del or Hm clones, or in all control clones (excluding non-translated pseudogenes). The overlap between differentially expressed proteins and *Csde1*-associated transcripts was limited to 29 transcripts (Fig. 4B, Supplementary Table S-V) suggesting that the differentially regulated proteins are primarily secondary targets of *Csde1*-controlled pathways. The only *Csde1*-associated transcript corresponding to a differentially expressed protein in both Del and Hm clones versus control clones is *Pabpc1* (*PolyA binding protein c1*; Supplementary Table V, see discussion).

RBPs such as *Csde1* control RNA stability and translation. To judge the role of *Csde1*, we generated RNA expression profiles, sequencing poly-adenylated RNA of the Del, Hm, and control MEL cells. Following normalization, we assessed the expression of *Csde1* in these clones. Expression of *Csde1* mRNA was reduced in clones D1, D2, H1 and H2, but also in clone C1, compared to C2 and parental MEL cells (Fig. 5A). A likelihood ratio test (LRT) followed by analysis of deviance by clone (ANODEV) was used to identify transcripts which differed significantly in expression across all samples. These transcripts were combined in a heatmap for all differentially expressed genes (Supplementary Figure S3; Supplementary Table S-VI). Strikingly, the RNAseq heatmap is very different from the proteome heatmap (Fig. 4A). In a PCA, the samples are poorly separated (Supplementary Figure S4a). The observed effect on protein expression suggests a potential role for *Csde1* on mRNA translation.

Correlation between protein and RNA expression of *Csde1*-bound transcripts. Correlation between mRNA abundance and protein expression among organisms and tissue types may be as low as 0.2–0.4^{30–36}. We investigated whether loss of *Csde1* alters the strength of correlation between mRNA and protein abundance for transcripts bound by *Csde1*. We calculated RPKM (Reads Per Kilobase of transcript per Million mapped reads) to quantify RNA expression, and normalized iBAQ values to quantify protein expression (Supplementary Table S-VII). Plotting Z-scores of RNA against protein expression visualized that both RNA and protein expression of *Csde1* were reduced in the MEL clones D1, D2, H1, H2 compared to low RNA and intermediate protein expression in clone C1 and increased RNA and protein expression in clones H2 and wt MEL cells (Fig. 5B). Looking broadly at all transcripts, the Spearman rank correlation coefficient between $^{10}\log(\text{RPKM})$ and $^{10}\log(\text{iBAQ})$ varied between 0.52 and 0.56 for all samples (Supplementary Table S-VIII). This is similar to the observed Pearson correlation of 0.59 between RNA and protein expression in two mouse hematopoietic cell lines³⁵. Surprisingly, the correlation coefficient differed only marginally for *Csde1*-bound transcripts compared to the transcript pool as a whole.

We also calculated the Pearson correlation coefficient between the Z scores of RNA (RPKM) and protein (iBAQ) for individual transcripts across conditions (Supplementary Table S-IX). The distribution of correlation coefficients showed that the strength of correlation can vary widely. The modal correlation coefficient between protein and RNA expression was 0.1, but there was no apparent difference between *Csde1*-bound transcripts (222) and random transcripts (6400; Fig. 5C).

Although *Csde1* does not influence the correlation between protein and mRNA for all its associated transcripts, it is possible that *Csde1* may regulate the balance of protein expression for a sub-selection of target transcripts. We focused on the *Csde1*-bound transcripts and plotted RNA expression against protein expression. Of particular interest is that *Csde1* target transcripts associated with protein degradation displayed distinct patterns of RNA and protein expression. Protein expression levels of the proteasome subunits *Psme1* ($r = 0.96$) and *Psmc3* ($r = -0.78$) were highly correlated and anti-correlated, respectively. Both RNA and protein expression of clones

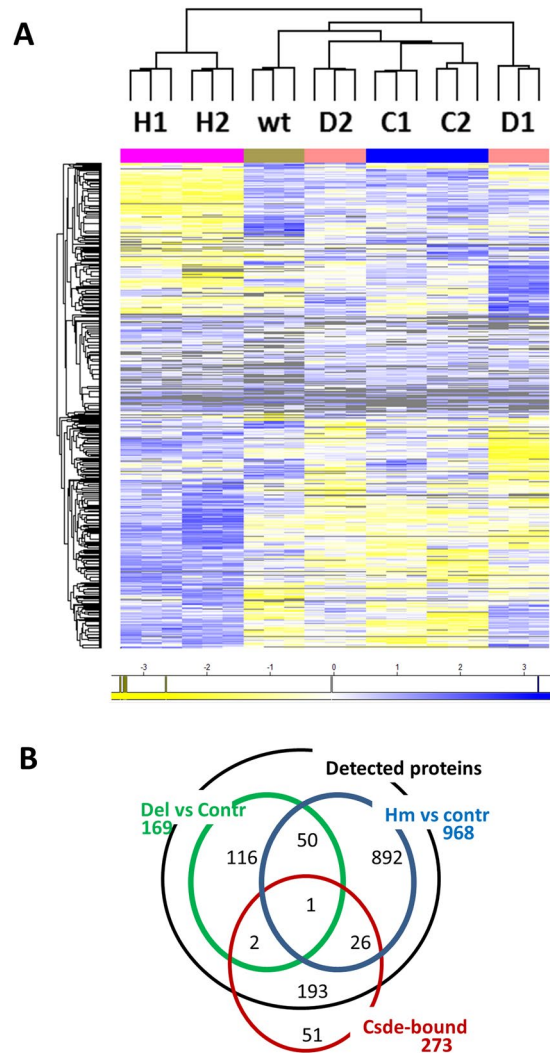


Figure 4. Proteome of *Csde1* deletion mutants. Total MEL cell lysates of 2 Hm clones (H1, H2), 2 Del clones (D1, D2), 2 clones with a heterozygous out-of-frame deletion (C1, C2), and the parental MEL cells (wt) were analysed by mass spectrometry. Three lysates were analysed for each clone. Data were analysed by MaxQuant and Perseus (A) Proteins differentially regulated between Hm and control clones (C1, C2 and wt), or between Del and control clones were subjected to Pearson clustering. (blue: upregulated, yellow: downregulated, grey: not detected). Proteins and their Z-score in the order of this heatmap are listed in Supplementary Table S-V. (B) The overlap between genes encoding proteins differentially expressed between Del and control clones (169, green circle); between Hm and control genes (968, blue circle) and genes encoding *Csde1*-bound transcripts of which proteins were detected by mass spectrometry (222, red circle) (FDR < 0.05).

D1, H1 and H2 were increased for *Psme1*, whereas for *Psmc3*, protein levels in these clones decreased while RNA levels increased (Fig. 6A,B). *Npepps* (*Aminopeptidase Puromycin Sensitive*) transcript levels of Del and Hm clones showed the same variation as control clones, but protein levels were increased, whereas RNA/protein relation was scattered for *Fkbp11* (*Fk506 Binding Protein 11*) (Fig. 6C,D).

Pabpc1 was the only protein encoded by a *Csde1*-bound transcript that was significantly changed in the Del and Hm clones compared to control clones (Fig. 4B). Interestingly, *Pabpc1* protein expression was increased whereas *Pabpc1* RNA expression was reduced in Del and Hm clones compared to control clones, which hints to feedback control (Fig. 6E, see discussion). In contrast, the splicing factors *Ddx18* (*Dead Box Polypeptide 18*) and *Vrk1* (*Vaccinia Related Kinase 1*) displayed lower protein expression from increased transcript levels in Del and Hm clones (Fig. 6F,G). *Csde1* was identified as being poorly translated in DBA, a ribosomopathy. Therefore, it is striking that three nucleolar proteins involved in ribogenesis (*Ebna1bp2*, *Ebna1 Binding Protein 2*; *Rpf2*, *Ribosome Production Factor 2*; *Nop56*, *nucleolar protein 56*) showed reduced protein expression in clones D1, H1 and H2 relative to controls whereas mRNA levels were similar (Fig. 6I-K). Additional transcripts with a clear segregation of Del and Hm clones versus control clones were *Blvra* (*Biliverdin Reductase A*), *Fam50a* (*Family With Sequence Similarity 50, Member A*), *Aldh2* (*Aldehyde Dehydrogenase 2*), *eIF3h* (*eukaryotic initiation factor 3h*), *Eprs* (*Glutamyl-Prolyl-Trna Synthetase*) and *Rps8* (*Ribosomal protein S8*) (Fig. 6H,L, Supplementary Figure S4B). In conclusion, reduced *Csde1* expression/function caused either increased or reduced protein expression. This

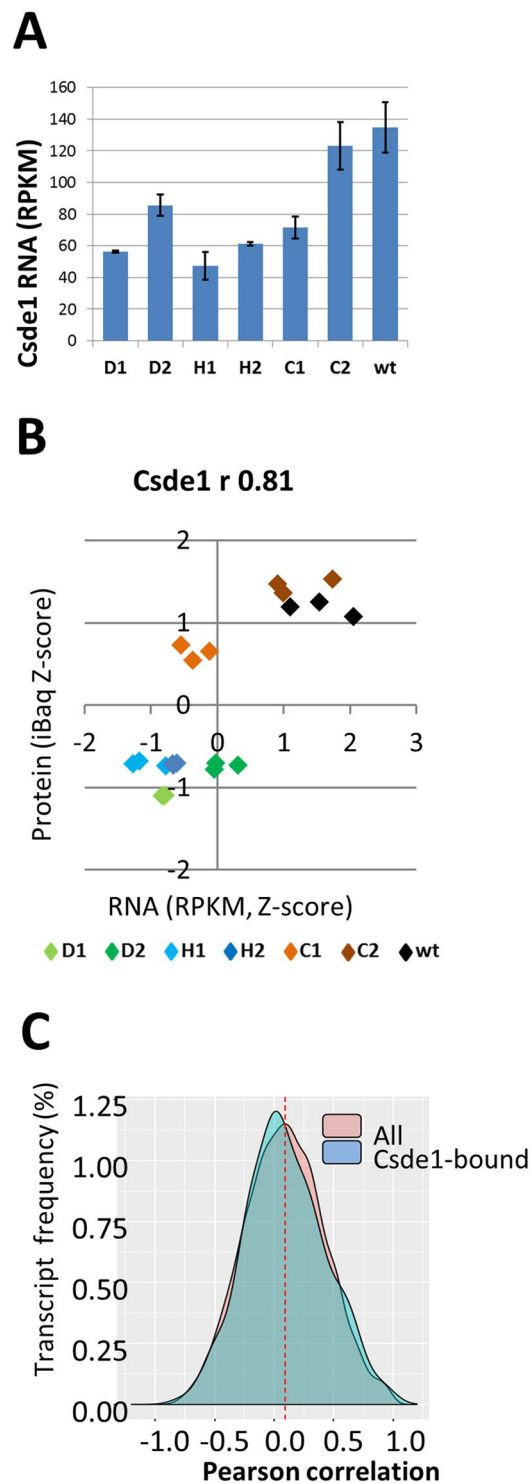


Figure 5. The correlation between protein and mRNA expression. RNA was isolated in triplicate from 2 Hm clones (H1, H2), 2 Del clones (D1, D2), 2 clones with a heterozygous out-of-frame deletion (C1, C2), and the parental MEL cells (wt), and polyAdenylated RNA was sequenced. RNA reads were normalized and calculated as RPKM (reads per kilobase per million). **(A)** RNA expression of Csde1 in RPKM. **(B)** The same cell isolates were used for RNA and protein analysis (Fig. 4). For each protein detected by mass spectrometry, the Pearson correlation (r) between protein (Z-scores of iBaq) and RNA (Z-scores of RPKM) was calculated for the 21 samples. The distribution of the correlation between -1 and $+1$ was plotted for all samples, and for transcripts bound by Csde1. **(C)** the correlation between protein and RNA was plotted for Csde (Z-scores, standard deviations from the mean). (Del clones: green; Hm clones: blue, HET control clones: orange-brown, wtMEL: black).

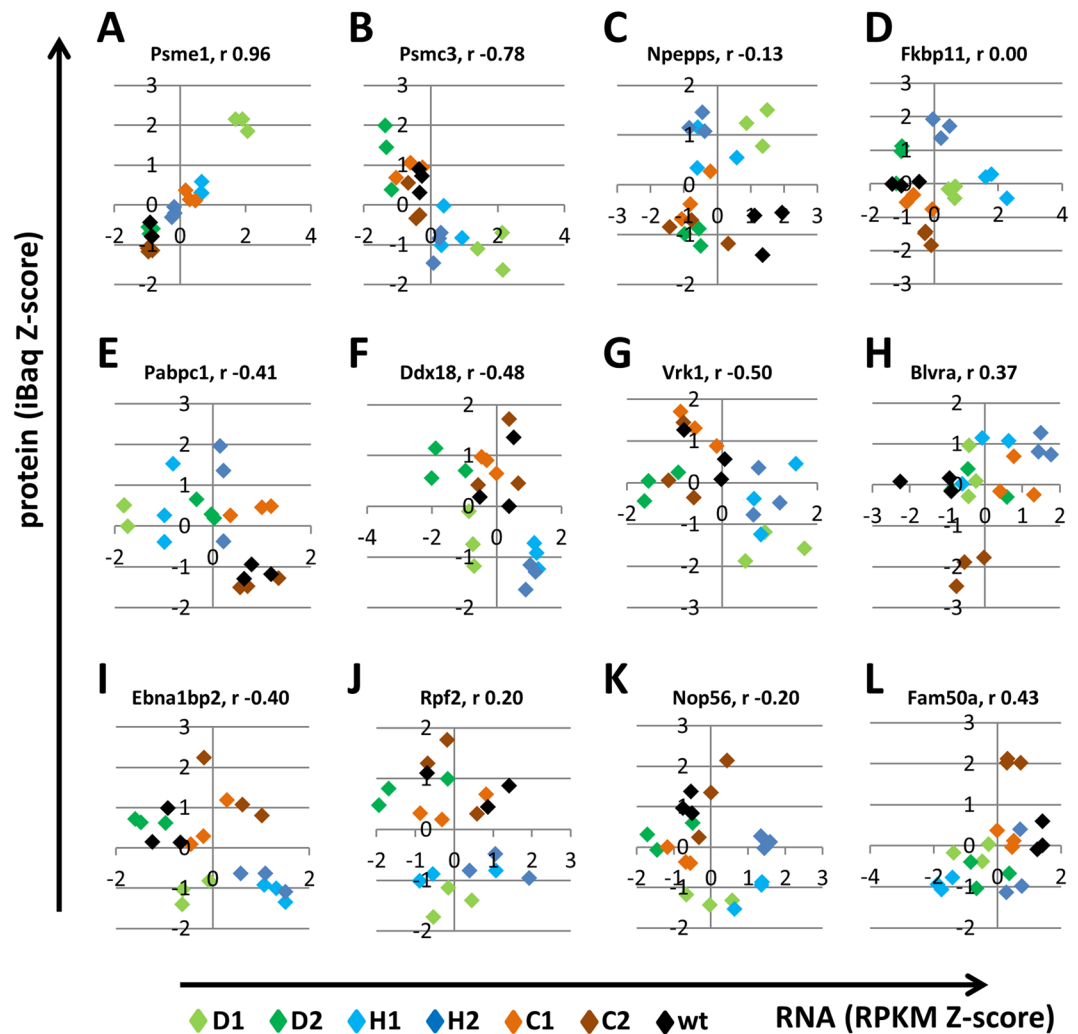


Figure 6. The correlation between protein and mRNA expression for few *Csde1*-bound transcripts. The correlation between protein and RNA was plotted for the indicated genes (Z-scores of iBaq and RPKM; see legend to Fig. 5). (Del clones: green; Hm clones: blue, HET control clones: brown, wtMEL: black).

suggests that the function of *Csde1* may be determined by the protein complex in which it acts on the fate of the bound transcript.

Effect of *Csde1* on erythroid specific transcripts. Finally, we investigated whether the effects of *Csde1* were erythroid specific, and whether *Csde1*-bound transcripts were involved in DBA because we identified *Csde1* as a transcript poorly translated in DBA⁴. The transcription factor Gata1 controls erythroid specific gene expression, and translation of Gata1 transcript is a hallmark of DBA³⁷. We compared the *Csde1*-associated transcripts with transcripts upregulated upon Gata1 activation in G1E cells³⁷ and found only 7 common targets: Hmbs (hydroxymethylbilane synthase; heme synthesis), Hagh (hydroxyacylglutathione hydrolase; antioxidant synthesis), Cdkn3 (cyclin dependent kinase inhibitor 3; CDK2 inhibitor), Atpif1 (ATPase inhibitory factor 1; mitochondrial protein), Napa (NSF attachment protein alpha; vesicle docking), Fam50a family with sequence similarity 50 member A; nuclear protein), and Arpc1a (actin related protein 2/3 complex subunit 1A; actin cytoskeleton). We also compared *Csde1*-bound targets with genes deregulated in erythroblasts derived from a mouse model for DBA suffering anemia³⁸. Only 9 targets were found in common, and none of those was a Gata1 target. They included Capzb (capping actin protein of muscle Z-line beta subunit; actin cytoskeleton), Fkbp11 (FK506 binding protein 11, protein folding, mTOR activity), Rpl14 (ribosomal protein L14), Mettl2 (methyltransferase like 2B), Rbms1 (RNA binding motif single stranded interacting protein 1), Mars (methionyl-tRNA synthetase), Phgdh (phosphoglycerate dehydrogenase; L-serine synthesis), Mtap (methylthioadenosine phosphorylase; salvage of methionine and adenosine), and Ostf1 (osteoclast stimulating factor 1). Given that we found 294 transcripts to be bound by *Csd1*, the overlap with Gata1 and DBA targets is limited. The 16 *Csde1*-bound transcripts that are reported as DBA and Gata targets do not include any of the 29 transcripts that show *Csde1*-dependent protein expression (Fig. 4B, Supplementary Table S-V).

Discussion

Csde1 is an RNA binding protein that is strongly upregulated during erythropoiesis, but its targets and the pathways controlled by Csde1 in erythropoiesis are unknown. We show that Csde1-bound transcripts in erythroblasts mainly encode proteins involved in ribogenesis, in mRNA translation and protein stability, and in mitochondrial function. Deletion of the N-terminal cold shock domain by Crispr/Cas9 resulted in truncated proteins due to in-frame deletions, or due to translation initiation downstream of out-of-frame deletions. The expression levels of mRNA and/or protein of multiple Csde1-bound transcripts were consistently changed in Csde1-mutated cells compared to control clones. Pabpc1 protein levels are increased, whereas the encoding mRNA is decreased. In contrast, the nucleolar ribogenesis factors Ebna1bp2, Rpf2, and Nop56 showed reduced protein expression in Del and Hm clones from comparable mRNA levels. The results suggest a general role for Csde1 in the regulation of transcript stability and translation, in addition to playing a role in protein homeostasis.

Csde1 binds mRNAs encoding proteins involved in ribogenesis and mitosis in the MEL cell line.

Defects in ribosomal proteins that are involved in ribosome biosynthesis cause DBA, a severe congenital anemia³⁹. Interestingly, mutations in the erythroid transcription factor *GATA1* also cause a DBA-like anemia^{40,41}, which suggests that at least a part of the *Gata1* target genes form a RNA regulon that is very sensitive to reduced ribosome availability⁴². *GATA1* itself is part of such a regulon because *GATA1* translation is reduced in erythroblasts of DBA patients³⁷. In mouse erythroblasts, *Gata1* translation is not affected upon reduced expression of DBA-related ribosomal proteins. Instead, we previously reported that translation of IRES (internal ribosomal entry site) containing transcripts is impaired under DBA conditions, and Csde1 was one of them⁴. This could be due to the less competitive nature of IRES-mediated recruitment of ribosomes to a transcript compared to cap-dependent ribosomal recruitment. This study reveals that Csde1 acts on a different subset of transcripts compared to the most prominent *Gata1* or DBA targets. However, Csde1 controls the same cellular pathways: ribogenesis and mRNA translation. Among the proteins involved in ribogenesis are Rpf2, Nop56 and Ebna1bp2^{43,44}. *Nop56* and *Ebna1bp2* also interacted with Csde1 in melanoma cells¹⁸. Expression of these proteins was reduced in Del and Hm clones. Rpf2 cooperates with Rpl5 and Rpl11 to incorporate 5S rRNA in the 60S ribosomal subunit. Of note, haploinsufficiency of RPL5 and RPL11 is a frequent cause of DBA. Nop56 is part of the Box C/D snoRNP complex and involved in rRNA methylation. Ebna1bp2 functions as a nucleolar scaffold protein. Two other proteins involved in ribosomal subunit maturation, Bola3 and Nol12, were bound by Csde1. However, their expression was too low for reliable detection by mass spectroscopy under the conditions used. Reduced efficacy of Csde1, and subsequent reduced expression of Rpf2, Nop56 and Ebna1bp2, is predicted to impair ribosome biogenesis^{45,46}. Further studies are needed to confirm the governing role of Csde1 on ribogenesis. The mechanism through which the reduction in Csde1 efficacy cooperates with haploinsufficiency of ribosomal proteins as observed in DBA is uncertain.

The identified Csde1-bound transcripts include 11 transcripts involved in cell cycle regulation, all of which encode proteins that function in mitosis. This includes centrosome-regulating proteins Aurkaip1 (Aurora kinase interacting protein), Ccdc77 (Coiled-Coil Domain Containing 77), Spc24 (Ndc80 Kinetochore Complex Component), and Tubgcp2 (Tubulin, Gamma Complex Associated Protein 2), whereas Actn4 (Actinin Alpha 4), Ccdc124 (Coiled-Coil Domain Containing 124), Cdkn3 (Cyclin-Dependent Kinase Inhibitor 3) and Tubgcp2 (Tubulin, Gamma Complex Associated Protein 2) control cytokinesis. Csde1 is known to control translation of Cdk11B (PITSLRE) during mitosis in HEK293 cells, which is IRES-driven and requires cooperation with hnRNP C1/C2¹¹. Expression of Cdk11 was not detected in erythroblasts using mass spectroscopy. We speculated previously that the occurrence of binucleated cells in erythroblasts that lack Rps19 (DBA-derived or upon knock down) is due to dysregulation of the centrosome or cytokinesis⁴. As polyribosome recruitment of Csde1 is diminished upon loss of Rps19, it is possible that disruption of Csde1 impairs cytokinesis via deregulation of these target proteins, resulting in a binucleated phenotype. This provides a possible mechanism for Csde1's role in DBA.

mRNA stability and translation of Csde1-bound transcripts. The Del and Hm clones displayed reduced *Pabpc1* mRNA expression, and increased Pabpc1 protein expression. Actually, *Pabpc1* was the only Csde1-bound transcript that was significantly deregulated in Del and Hm clones. *Pabpc1* is an important target because it enhances both mRNA stability and translation in general. Pabpc1 binds the polyA tail of transcripts, which protects them from deadenylation and subsequent degradation⁴⁷. Pabpc1 simultaneously binds eIF4G scaffold of the cap-binding complexes which loops the polyA tail of a transcript to the start of the transcript and is supposed to enhance reassociation of ribosomal subunits for a new round of translation⁴⁸. In addition, Pabpc1 is involved in ribonucleoprotein complexes that regulate the stability or translation of distinct transcripts. Csde1/UNR was shown to cooperate with Pabp in the combined regulation of mRNA stability and translation of several transcripts using distinct mechanisms^{16,17,49–51}. Most importantly, Csde1/UNR forms a complex with Pabpc1 and Imp1 that binds an adenine-rich autoregulatory sequence (ARS) in the 5'UTR of *Pabp*. The ability of mutated ARS sequences to bind the trimeric UNR/Imp/Pabp complex correlated with their repression of *Pabp* translation⁵², though it was not shown in their report that reduced Csde1/UNR expression affected *Pabp* expression. The existence of this trimeric complex predicts that loss of Csde1 function will increase protein expression of Pabpc1, as we observed. Increased Pabp levels may mitigate the repression, which would limit the effects of reduced Csde1 function.

Truncated Csde1 proteins expressed in deletion mutants. Whereas the Csde1-bound transcripts and encoded proteins show relatively small differences in expression levels, the overall proteome is vastly different. Strikingly, the Hm clones are much alike, but different from the Del clones. It was surprising that mass spectrometry detected Csde1 peptides in MEL clones harboring a Cas9-induced out-of-frame deletion. The deletion we aimed at started within the first tryptic peptide of Csde1 encoded by exon 3, and spans 5 tryptic peptides to end

within the first tryptic peptide encoded by exon 4. Three of these peptides are detected in the control clones, but not in the clones harboring a deletion. Moreover, we only detect smaller proteins in de MEL clones harboring a deletion. These proteins most likely arose from alternative start codon recognition. The 5'UTR of *Csde1* harbors several translated uORFs, which enables skipping of the first AUG start codon^{28,29}, and translation initiation at downstream start codons in a favorable Kozak consensus sequence. These are present at the end of exon 4 (the same exon that is targeted for the deletion), and in exon 6 (Fig. 3E). Complete loss of *Csde1* is not compatible with embryonic development⁵³, and *Csde1* has a pLI score of 1.0 in the Exome Aggregation Consortium database⁵⁴, indicating an extreme intolerance for Loss of Function (LoF) mutations. One recent study has found that cold shock domains 2 and 4 are the only cold shock domains required (out of 5) for translational stimulation⁵⁰, though there is also evidence to suggest that all five cold shock domains contribute to the ability of *Csde1* to stimulate translation, especially from IRESs²⁶. The data strongly suggest that MEL cells carrying an out-of-frame deletion underwent selection to maximize leaky scanning. This change in translation initiation efficiency will change the entire proteome, as approximately 50% of all transcripts carries an uORF, which renders protein expression dependent on the rate of leaky scanning (manuscript in preparation)^{29,55,56}.

The Crispr/Cas9-induced in frame deletion is not expected to affect transcript levels. The out-of-frame deletion, however, is expected to cause nonsense-mediated decay (NMD) due to splice factors residing at the many downstream splice junction sites⁵⁷. The Hm clones may carry an in-frame deleted allele (Fig. 3B), and an out-of-frame deletion that is lost due to NMD. This could explain the lower expression in the Hm clones compared to the parental MEL cells. Importantly, the Del clones were expressed at similar levels as Hm clones, the expression was not lost due to NMD. This is in accordance with the proposed leaky scanning and translation of a shorter *Csde1* protein isoform, which would protect the *Csde1* transcript from NMD. Of note, the first in frame AUG codon downstream of the deletion occurs in exon 4, between the deletion and the first splice junction that could give rise to NMD (Fig. 3E).

Materials and Methods

Cell culture. Murine erythroleukemia (Mel) and HEK293T cells were cultured in RPMI, and DMEM respectively (ThermoFisher), supplemented with 10% (vol/vol) fetal calf serum (FCS; Bodinco), glutamine and Pen-Strep (ThermoFisher). Mel cells expressing BirA, or BirA plus biotag-*Csde1* were described previously⁴. Cell number and size were determined using CASY cell counting technology (Roche).

Lentivirus production and transductions. HEK293Ts were transfected with pLKO.1-puro lentiviral construct containing shRNA sequences for *Csde1*: TRCN0000181609 and a scrambled control shRNA: SHC002 (MISSION TRC-Mm 1.0 shRNA library; Sigma-Aldrich; available on the BloodWeb site), pMD2.G, and pSPAX.2 packaging plasmids (as described before⁴) using 0.5M CaCl₂ and HEPES (ThermoFisher). 72 hours after transduction, viral supernatant was harvested and concentrated using 5% w/v PEG8000 (Sigma). Mel cells were transduced with a multiplicity of infection of 3–5 and addition of 8 µg/mL of Polybrene (Sigma-Aldrich). Transduced cells were selected with 1 µg/ml puromycin 24 hours after transduction.

Protein-RNA pulldown for *Csde1*. 100 million Mel-BirA and Mel-BirA-*Csde1*-tag cells were subjected to RNA immunoprecipitation using the protocol described by Keene *et al.*⁵⁸, with the following modifications. M-270 Dynabeads (ThermoFisher) were utilized in a volume of 100 µl per 100 million cells. The Dynabeads were blocked for 1 hour at 4 °C in 5% chicken egg albumin and then washed 3x in ice-cold NT2 buffer consisting of 50 mM Tris-HCl (Sigma-Aldrich), 150 mM NaCl (Sigma-Aldrich), 1 mM MgCl₂ (ThermoFisher) and 0.05% NP40 (Sigma-Aldrich) prior to use. The beads were then resuspended in 850 µl cold NT2, supplemented by 200U RNase Out (EMD Bioscience), 400 µM vanadyl ribonucleoside complexes (VRC, New England Biolabs) and 20 mM EDTA (EM Science). Incubation was done for 2 hours at 4 °C. The beads were then immobilized in a magnet rack and washed 5x with NT2 in 0.3M NaCl. At this point, the beads were split into a protein and an RNA fraction. The protein fraction was eluted via boiling in 1× Laemmli buffer (Sigma-Aldrich) for 5 minutes. RNA fractions were purified using Trizol (Invitrogen), precipitated in isopropanol and washed in 75% ethanol.

SDS-PAGE and Western blotting. Proteins were detected via SDS-PAGE and Western blotting as described in Horos *et al.*⁴. Antibodies used were directed against *Csde1* (NBP1-71915, Novus Biological), Actin (A3853, Sigma-Aldrich) and alpha Tubulin (ab4074, Abcam). Fluorescently labeled secondary antibodies for visualization with Odyssey were IRDye 680RD Donkey anti-Rabbit IgG (926–68073, Licor) and IRDye 800CW Donkey anti-Mouse IgG (925–32212, Licor).

cDNA synthesis and qRT-PCR. cDNA was generated from 1 µg RNA, using 1 µg random primers (48190011, Invitrogen), 50U M-MLV reverse transcriptase (Invitrogen), 1 mM dNTPs (Invitrogen) in M-MLV reverse transcriptase buffer (Invitrogen) supplemented with 5 mM DTT (ThermoFisher). The cDNA mix was heated for 45' at 42 °C and then for 3' at 99 °C.

Q-RT-PCR was performed as described in Horos *et al.*⁴, with the following modifications. A master mix was created using 10 µM of each primer, 12.5 µl SYBR Green master mix (4309155, Applied Biosystems) and 5 µl cDNA filled to a final concentration of 20 µl. Primers can be found in Supplementary Table S-I.

Mass spectrometry. Eluted peptides were processed as described by⁵⁹. Samples were subjected to mass spectrometry using label-free quantification. All data was analyzed and processed with MaxQuant for peptide identification and quantification²⁷. Downstream statistical analysis was performed with Perseus v1.5.1.6⁶⁰. All proteins matching the reverse database, potential contaminants, and those only identified by site were filtered out. To be considered for analysis, a protein had to be detectable within all triplicates of at least one clone. Prior to statistical testing, a log₂ transformation was performed. Because failures to detect a given peptide is sometimes

due to insufficient depth, missing values were imputed from the normal distribution with a width of 0.3 and a downshift of 1.8. These values were later de-imputed prior to visualization and production of the final tables. For multi-way ANOVA between CRISPR clones, an artificial within-group variance (S_0) threshold of 0.4 was used⁶¹. For two-way comparisons between groups, a *t*-test with a threshold of $S_0 = 0.5$ was used. For all analyses, a Benjamini-Hochberg false discovery rate of <0.05 was applied.

Production of Csde1 CRISPR clones. Guide RNAs for Csde1 were designed using an online web tool from the Massachusetts Institute of Technology (<http://crispr.mit.edu/>). The probes were designed to target the sequences upstream and downstream of the first cold shock domain and selected on the basis of faithfulness to on-target activity (Supplementary Table S1). CRISPR clones were generated as described in Cong *et al.*²⁵. Briefly, the guide RNAs were ligated in the PX458 Cas9 expression vector and electroporated into Mel cells with the Amaxa SFC cell line 4D-nucleofector XkitL. GFP positive cells were sorted using flow cytometry and deleted regions were checked using genotyping primers (Supplementary Table S1), Sanger sequencing and Western blotting.

Seahorse. Mitochondrial respiration levels for Csde1 CRISPR clones were determined on Seahorse XF96 using the Seahorse XF Mito Stress Test kit. 24 hours prior to the assay, cells were seeded at a concentration of 150,000 in 500 μ l RPMI on a XF cell culture microplate. One hour before measurement, medium was replaced by DMEM (Sigma, D5030) containing 25 mM glucose (Sigma), 1 mM sodium pyruvate (Lonza), and 2 mM L-glutamine (Life technologies) and cells were incubated in a non-CO₂ 37C incubator. Basal oxygen consumption rate (OCR) was detected as an indicator of mitochondrial respiration. OCR was measured in response to injection of oligomycin (15 μ M), FCCP (1 μ M), antimycin A (2.5 μ M) and rotenone (1.25 μ M). Experiments were performed in triplicate with 8 or 9 wells per experiment.

RNA-sequencing. RNA-seq on RNA immunoprecipitated with Csde1 was performed by the Leiden Genome Technology Center (LGTC, Leiden), using library preparation following the template-switch protocol (Clontech) followed by Nextera tagmentation. These samples were pooled together on one miSeq (Illumina) lane (2×150 bp, paired end). Sequence quality was checked using Fastqc (Babraham Bioinformatics). Quality control and trimming was performed using Trimmomatic with the following parameters: LEADING 20, TRAILING 20, SLIDINGWINDOW 4:20, MINLEN:50. We then used Tophat v2.0.9⁶² to align to mouse genome mm10 (Dec 2011) using the following parameters: library-type fr-unstranded,-mate-inner-dist 50,-mate-std-dev 20. The resulting bam files were sorted and indexed using samtools. Read count tables were produced using HTseq count⁶³ in conjunction with a mouse mm10 gtf downloaded from the UCSC browser on 14 March 2014.

RNA expression by total mRNA sequencing from Csde1 CRISPR clones was performed by Novogene Co., LTD. Briefly, library preparation was performed using the NEB Next[®] Ultra[™] RNA Library Prep Kit and enriched using oligo(dT) beads. Isolated mRNA was fragmented randomly in fragmentation buffer, followed by cDNA synthesis using random hexamers and reverse transcriptase. After first-strand synthesis, a custom second-strand synthesis buffer (Illumina) was added with dNTPs, RNase H and Escherichia coli polymerase I to generate the second strand by nick-translation. The final cDNA library is ready after a round of purification, terminal repair, A-tailing, ligation of sequencing adapters, size selection and PCR enrichment. The complete library was sequenced using Illumina HiSeq. 2500 (2×150 bp, paired end). Sequence quality was checked using Fastqc (Babraham Bioinformatics). Spliced Transcripts Alignment to a Reference (STAR⁶⁴) was used to align the sequences to the mouse mm10 genomic reference sequence, using the following parameters: -outFilterMultimapNmax 20,-outFilterMismatchNmax 1,-outSAMmultNmax 1,-outSAMtype BAM SortedByCoordinates, quant-Mode GeneCounts, -outWigType wiggle, -outWigStrand Stranded,-outWigNorm RPM. A gtf file accessed from the UCSC genome browser on 11-Sept-2015 was passed to STAR using -sjdbGTFfile.

In both experiments, the read count tables were subjected to differential expression analysis with DESeq2⁶⁵. DESeq2 implements a negative binomial generalized linear model to identify differential expressed/enriched transcripts. This method normalizes raw counts by adjusting for a size factor to account for discrepancies in sequencing depth between samples. The normalized counts are subsequently subjected to a Wald test with a Benjamini-Hochberg (FDR) correction for multiple testing, or a likelihood ratio test followed by analysis of deviance, in the case of multi-sample comparisons. DESeq2 also provides a function for principle component analysis (PCA). Additional visualizations were made using R packages ggplots, dheatmap and pheatmap. Overrepresentation Analysis (ORA) for GO-terms and pathways was performed on significant transcripts with GeneTrail²³.

Identification of Csde1 binding sites in target transcripts. A custom Python script using Biopython was created to search transcripts for Csde1 binding sites²². Briefly, the script parses Genbank sequences into a Python dictionary and then scans the transcript for the presence of one of the known binding sites represented as regular expressions. Using the Genbank annotation, the script reports the location and exact sequence of the potential binding site(s). The script is available as Supplementary Information.

Correlation of RNA and protein expression levels. To determine the degree to which RNA expression determines protein abundance, we calculated a Pearson correlation coefficient between the Z-scores from RNA sequencing and mass spectrometry data for each gene. Z-scores were calculated after normalization: In mass spectrometry, iBAQ values as determined via MaxQuant were normalized via a scaling factor calculated by dividing the sum of intensities from each sample by the intensity sum of a reference sample. RNA expression levels were normalized as reads per kilobase of transcript per million mapped reads (RPKM). When performing a sample-wise correlation between mRNA and protein expression, we utilized a Spearman rank correlation coefficient between $^{10}\log(\text{RPKM})$ and $^{10}\log(\text{iBAQ})$.

Accession numbers. Original sequencing results have been deposited in the BioProject Database under project ID PRJNA378565. The mass spectrometry proteomics data have been deposited to the ProteomeXchange Consortium via the PRIDE partner repository with the dataset identifier PXD006358.

References

- Keene, J. D. RNA regulons: coordination of post-transcriptional events. *Nat. Rev. Genet.* **8**, 533–543 (2007).
- de Andrés-Aguayo, L., Varas, F. & Graf, T. Musashi 2 in hematopoiesis. *Curr. Opin. Hematol.* **19**, 268–272 (2012).
- Zhang, L. *et al.* ZFP36L2 is required for self-renewal of early burst-forming unit erythroid progenitors. *Nature* **499**, 92–6 (2013).
- Horos, R. *et al.* Ribosomal deficiencies in Diamond-Blackfan anemia impair translation of transcripts essential for differentiation of murine and human erythroblasts. *Blood* **119**, 262–72 (2012).
- Jacquemin-Sablon, H. *et al.* Nucleic acid binding and intracellular localization of unr, a protein with five cold shock domains. *Nucleic Acids Res.* **22**, 2643–50 (1994).
- Cornelis, S., Tinton, S. A., Schepens, B., Bruynooghe, Y. & Beyaert, R. UNR translation can be driven by an IRES element that is negatively regulated by polypyrimidine tract binding protein. *Nucleic Acids Res.* **33**, 3095–108 (2005).
- Abaza, I., Coll, O., Patalano, S. & Gebauer, F. Drosophila UNR is required for translational repression of male-specific lethal 2 mRNA during regulation of X-chromosome dosage compensation. *Genes Dev.* **20**, 380–9 (2006).
- Dormoy-Raquet, V., Markovits, J., Jacquemin-Sablon, A. & Jacquemin-Sablon, H. Regulation of Unr expression by 5'- and 3'- untranslated regions of its mRNA through modulation of stability and IRES mediated translation. *RNA Biol.* **2**, e27–35 (2005).
- Mitchell, S. A., Spriggs, K. A., Coldwell, M. J., Jackson, R. J. & Willis, A. E. The Apaf-1 internal ribosome entry segment attains the correct structural conformation for function via interactions with PTB and unr. *Mol. Cell* **11**, 757–71 (2003).
- Zhang, C. *et al.* Hepsin inhibits CDK11p58 IRES activity by suppressing unr expression and eIF-2 α phosphorylation in prostate cancer. *Cell. Signal.* **27**, 789–97 (2015).
- Schepens, B. *et al.* A role for hnRNP C1/C2 and Unr in internal initiation of translation during mitosis. *EMBO J.* **26**, 158–69 (2007).
- Anderson, E. C. & Catnaigh, P. Ó. Regulation of the expression and activity of Unr in mammalian cells. *Biochem. Soc. Trans.* **43**, (2015).
- Ray, S., Catnaigh, P. Ó. & Anderson, E. C. Post-transcriptional regulation of gene expression by Unr. *Biochem. Soc. Trans.* **43** (2015).
- Bushell, M. *et al.* Polypyrimidine Tract Binding Protein Regulates IRES-Mediated Gene Expression during Apoptosis. *Mol. Cell* **23**, 401–412 (2006).
- Kamenska, A. *et al.* The DDX6-4E-T interaction mediates translational repression and P-body assembly. *Nucleic Acids Res.* **44**, 6318–34 (2016).
- Duncan, K. E., Strein, C. & Hentze, M. W. The SXL-UNR Corepressor Complex Uses a PABP-Mediated Mechanism to Inhibit Ribosome Recruitment to msl-2 mRNA. *Mol. Cell* **36**, 571–582 (2009).
- Chang, T. C. *et al.* UNR, a new partner of poly(A)-binding protein, plays a key role in translationally coupled mRNA turnover mediated by the c-fos major coding-region determinant. *Genes Dev.* **18**, 2010–2023 (2004).
- Wurth, L. *et al.* UNR/CSDE1 Drives a Post-transcriptional Program to Promote Melanoma Invasion and Metastasis. *Cancer Cell* **30**, 694–707 (2016).
- Huang, C.-C. *et al.* Concurrent gene signatures for han chinese breast cancers. *PLoS One* **8**, e76421 (2013).
- de Boer, E. *et al.* Efficient biotinylation and single-step purification of tagged transcription factors in mammalian cells and transgenic mice. *Proc. Natl. Acad. Sci. USA* **100**, 7480–5 (2003).
- Trigueneaux, G., Velten, M., Franzone, P., Dautry, F. & Jacquemin-Sablon, H. RNA binding specificity of Unr, a protein with five cold shock domains. *Nucleic Acids Res.* **27**, 1926–34 (1999).
- Cock, P. J. A. *et al.* Biopython: freely available Python tools for computational molecular biology and bioinformatics. *Bioinformatics* **25**, 1422–1423 (2009).
- Stöckel, D. *et al.* Multi-omics enrichment analysis using the GeneTrail2 web service. *Bioinformatics* **32**, 1502–1508 (2016).
- Mihalovic, M. *et al.* Widespread generation of alternative UTRs contributes to sex-specific RNA binding by UNR. *RNA* **18**, 53–64 (2012).
- Cong, L. *et al.* Multiplex genome engineering using CRISPR/Cas systems. *Science* **339**, 819–23 (2013).
- Brown, E. C. & Jackson, R. J. All five cold-shock domains of unr (upstream of N-ras) are required for stimulation of human rhinovirus RNA translation. *J. Gen. Virol.* **85**, 2279–2287 (2004).
- Cox, J. & Mann, M. MaxQuant enables high peptide identification rates, individualized p.p.b.-range mass accuracies and proteome-wide protein quantification. *Nat. Biotechnol.* **26**, 1367–1372 (2008).
- Michel, A. M. *et al.* GWIPS-viz: development of a ribo-seq genome browser. *Nucleic Acids Res.* **42**, D859–D864 (2014).
- de Klerk, E. *et al.* Assessing the translational landscape of myogenic differentiation by ribosome profiling. *Nucleic Acids Res.* **43**, 4408–28 (2015).
- Maier, T., Güell, M. & Serrano, L. Correlation of mRNA and protein in complex biological samples. *FEBS Lett.* **583**, 3966–3973 (2009).
- Ingolia, N. T., Ghaemmaghami, S., Newman, J. R. S. & Weissman, J. S. Genome-wide analysis *in vivo* of translation with nucleotide resolution using ribosome profiling. *Science* **324**, 218–23 (2009).
- Lundberg, E. *et al.* Defining the transcriptome and proteome in three functionally different human cell lines. *Mol. Syst. Biol.* **6**, 450 (2010).
- Vogel, C. & Marcotte, E. M. Insights into the regulation of protein abundance from proteomic and transcriptomic analyses. *Nat. Rev. Genet.* **13**, 227–32 (2012).
- Vogel, C. *et al.* Sequence signatures and mRNA concentration can explain two-thirds of protein abundance variation in a human cell line. *Mol. Syst. Biol.* **6**, 400 (2010).
- Tian, Q. *et al.* Integrated genomic and proteomic analyses of gene expression in Mammalian cells. *Mol. Cell. Proteomics* **3**, 960–9 (2004).
- Schwanhäusser, B. *et al.* Global quantification of mammalian gene expression control. *Nature* **473**, 337–342 (2011).
- Ludwig, L. S. *et al.* Altered translation of GATA1 in Diamond-Blackfan anemia. *Nat. Med.* <https://doi.org/10.1038/nm.3557> (2014).
- Gazda, H. T. *et al.* Ribosomal protein L5 and L11 mutations are associated with cleft palate and abnormal thumbs in Diamond-Blackfan anemia patients. *Am. J. Hum. Genet.* **83**, 769–80 (2008).
- Vlachos, A., Blanc, L. & Lipton, J. M. Diamond Blackfan anemia: a model for the translational approach to understanding human disease. *Expert Rev. Hematol.* **7**, 359–372 (2014).
- Sankaran, V. G. *et al.* Exome sequencing identifies GATA1 mutations resulting in Diamond-Blackfan anemia. *J. Clin. Invest.* **122**, 2439–43 (2012).
- Parrella, S. *et al.* Loss of GATA-1 full length as a cause of Diamond-Blackfan anemia phenotype. *Pediatr. Blood Cancer* **61**, 1319–21 (2014).
- Paolini, N. A. *et al.* In *eLS* 1–8 (John Wiley & Sons, Ltd, 2016). <https://doi.org/10.1002/9780470015902.a0024471>.
- van Nues, R. W. *et al.* Box C/D snoRNP catalysed methylation is aided by additional pre-rRNA base-pairing. *EMBO J.* **30**, 2420–30 (2011).

44. Hirano, Y. *et al.* Proteomic and targeted analytical identification of BXDC1 and EBNA1BP2 as dynamic scaffold proteins in the nucleolus. *Genes to Cells* **14**, 155–166 (2009).
45. Asano, N. *et al.* Structural and functional analysis of the Rpf2-Rrs1 complex in ribosome biogenesis. *Nucleic Acids Res.* **43**, 4746–57 (2015).
46. Asano, N. *et al.* Crystallization and preliminary X-ray crystallographic analysis of ribosome assembly factors: the Rpf2-Rrs1 complex. *Acta Crystallogr. Sect. F, Struct. Biol. Commun.* **70**, 1649–52 (2014).
47. Gray, N. K., Hrabálková, L., Scanlon, J. P. & Smith, R. W. P. Poly(A)-binding proteins and mRNA localization: who rules the roost? *Biochem. Soc. Trans.* **43**, (2015).
48. Kedersha, N. & Anderson, P. In *Methods in enzymology* **431**, 61–81 (2007).
49. Patel, G. P. & Bag, J. IMP1 interacts with poly(A)-binding protein (PABP) and the autoregulatory translational control element of PABP-mRNA through the KH III-IV domain. *FEBS J.* **273**, 5678–5690 (2006).
50. Ray, S. & Anderson, E. C. Stimulation of translation by human Unr requires cold shock domains 2 and 4, and correlates with poly(A) binding protein interaction. *Sci. Rep.* **6**, 22461 (2016).
51. Grosset, C. *et al.* A mechanism for translationally coupled mRNA turnover: interaction between the poly(A) tail and a c-fos RNA coding determinant via a protein complex. *Cell* **103**, 29–40 (2000).
52. Patel, G. P., Ma, S. & Bag, J. The autoregulatory translational control element of poly(A)-binding protein mRNA forms a heteromeric ribonucleoprotein complex. *Nucleic Acids Res.* **33**, 7074–89 (2005).
53. Mihailovich, M., Militti, C., Gabaldón, T. & Gebauer, F. Eukaryotic cold shock domain proteins: highly versatile regulators of gene expression. *Bioessays* **32**, 109–18 (2010).
54. Lek, M. *et al.* Analysis of protein-coding genetic variation in 60,706 humans. *Nature* **536**, 285–291 (2016).
55. Matsui, M., Yachie, N., Okada, Y., Saito, R. & Tomita, M. Bioinformatic analysis of post-transcriptional regulation by uORF in human and mouse. *FEBS Letters* **581** (2007).
56. Iacono, M., Mignone, F. & Pesole, G. uAUG and uORFs in human and rodent 5′ untranslated mRNAs. *Gene* **349**, 97–105 (2005).
57. Karousis, E. D., Nasif, S. & Mühlemann, O. Nonsense-mediated mRNA decay: novel mechanistic insights and biological impact. *Wiley Interdiscip. Rev. RNA* **7**, 661–682 (2016).
58. Keene, J. D., Komisarow, J. M. & Friedersdorf, M. B. RIP-Chip: the isolation and identification of mRNAs, microRNAs and protein components of ribonucleoprotein complexes from cell extracts. *Nat. Protoc.* **1**, 302–307 (2006).
59. Gazendam, R. P. *et al.* Impaired killing of *Candida albicans* by granulocytes mobilized for transfusion purposes: a role for granule components. *Haematologica* **101**, 587–96 (2016).
60. Tyanova, S. *et al.* The Perseus computational platform for comprehensive analysis of (prote)omics data. *Nat. Methods* **13**, 731–740 (2016).
61. Tusher, V. G., Tibshirani, R. & Chu, G. Significance analysis of microarrays applied to the ionizing radiation response. *Proc. Natl. Acad. Sci. USA* **98**, 5116–21 (2001).
62. Kim, D. *et al.* TopHat2: accurate alignment of transcriptomes in the presence of insertions, deletions and gene fusions. *Genome Biol.* **14**, R36 (2013).
63. Anders, S., Pyl, P. T. & Huber, W. HTSeq—a Python framework to work with high-throughput sequencing data. *Bioinformatics* **31**, 166–169 (2015).
64. Dobin, A. *et al.* STAR: ultrafast universal RNA-seq aligner. *Bioinformatics* **29**, 15–21 (2013).
65. Love, M. I., Huber, W. & Anders, S. Moderated estimation of fold change and dispersion for RNA-seq data with DESeq2. *Genome Biol.* **15**, 550 (2014).

Acknowledgements

We want to thank Ben Nota for ICT support and Monika Wolkers for critical reading of the manuscript. Additionally, we would like to thank Klaske Thiadens, Fiamma Salerno, Franca di Summa and Aicha Ait Soussan for their support and expertise in the laboratory setting. This work was supported by the Landsteiner Foundation for Bloodtransfusion Research (LSBR) [projects 1140 and 1239 to MvL, and fellowship 1238 to EvdA].

Author Contributions

K.S.M., N.Y., F.v.A., N.A.P., R.H., and N.M.H. prepared and executed laboratory experiments. K.S.M. and M.v.L. were responsible for strategic experimental design, consulting with P.A.C.tH., E.v.d.A., A.B.M., and R.H.H. for experiments relevant to their areas of expertise. K.S.M., M.v.L., E.v.d.A., A.B.M., R.H.H., and P.A.C.tH. collaborated to analyze and interpret results relevant to personal areas of expertise. K.S.M. wrote the requisite Python and R code with guidance from P.A.C.tH. Manuscript text was written by K.S.M. and M.v.L. All authors reviewed the manuscript.

Additional Information

Supplementary information accompanies this paper at <https://doi.org/10.1038/s41598-018-20518-7>.

Competing Interests: The authors declare no competing interests.

Publisher's note: Springer Nature remains neutral with regard to jurisdictional claims in published maps and institutional affiliations.



Open Access This article is licensed under a Creative Commons Attribution 4.0 International License, which permits use, sharing, adaptation, distribution and reproduction in any medium or format, as long as you give appropriate credit to the original author(s) and the source, provide a link to the Creative Commons license, and indicate if changes were made. The images or other third party material in this article are included in the article's Creative Commons license, unless indicated otherwise in a credit line to the material. If material is not included in the article's Creative Commons license and your intended use is not permitted by statutory regulation or exceeds the permitted use, you will need to obtain permission directly from the copyright holder. To view a copy of this license, visit <http://creativecommons.org/licenses/by/4.0/>.

© The Author(s) 2018